Reduced dynamics with renormalization in solid-state charge qubit measurement



2009 J. Phys.: Condens. Matter 21 385801

(http://iopscience.iop.org/0953-8984/21/38/385801)

J. Phys.: Condens. Matter **21** (2009) 385801 (5pp) doi:10.1088/0953-8984/21/38/385801

# Reduced dynamics with renormalization in solid-state charge qubit measurement

**Jun Yan Luo[1], Hujun Jiao[2], Feng Li[2], Xin-Qi Li[1,2,3] and Yi Jing Yan[1]**

[1] Department of Chemistry, Hong Kong University of Science and Technology, Kowloon, Hong Kong
[2] State Key Laboratory for Superlattices and Microstructures, Institute of Semiconductors, Chinese Academy of Sciences, PO Box 912, Beijing 100083, People's Republic of China
[3] Department of Physics, Beijing Normal University, Beijing 100875, People's Republic of China

Received 17 May 2009, in final form 11 August 2009
Published 27 August 2009
Online at stacks.iop.org/JPhysCM/21/385801

**Abstract**
Quantum measurement will inevitably cause backaction on the measured system, resulting in the well-known dephasing and relaxation. In this paper, in the context of solid-state qubit measurement by a mesoscopic detector, we show that an alternative backaction known as *renormalization* is important under some circumstances. This effect is largely overlooked in the theory of quantum measurement.

## 1. Introduction

One of the key requirements for physically implementing quantum computation is the ability to read out a two-state quantum system (qubit). Among various proposals, an important one is to use an electrometer as a detector whose conductance depends on the charge state of a nearby qubit. Such an electrometer can be a quantum point contact (QPC) [1–8] or a single-electron transistor [9–16]. Both of them have been preliminarily implemented in experiments for quantum measurements [17–21]. Also, similar structures were proposed for entanglement generation and detection by conduction electrons [22–24].

The problem of measuring a charge qubit by a QPC detector has been well studied in the high bias voltage regime. Work for arbitrary measurement voltage has also been reported although relatively limited [8, 25]. Most of them only dealt with the measurement-induced dephasing and relaxation, which, from the perspective of information, are consequences of information acquisition by measurement. The physical interaction between the measurement apparatus and the qubit, however, gives rise to another important backaction which renormalizes the internal structure of qubit.

In this context, we revisit the measurement problem, while taking fully into account the energy renormalization. This effect was often disregarded in the literature. Indeed, the steady-state renormalization can be effectively included in the Caldeira–Leggett renormalized system Hamiltonian [26–29]. The resulting dynamics is, however, different in detail from that of the dynamical renormalization approach [26, 27]. The apparent distinction should be sensitively reflected in the output power spectral density studied in this work. Our analysis shows that the renormalization effect on qubits becomes increasingly important as one lowers the measurement voltage. Therefore, it would require us in practice to have this feature being taken into account properly in order to correctly analyze and understand the measurement results.

## 2. Model description

The system under investigation is schematically shown in figure 1. The Hamiltonian of the entire system is of $H_{\rm T} = H_{\rm qu} + H_{\rm D} + H'$, with the qubit, QPC detector and their coupling parts being modeled respectively by

$$H_{\rm qu} = \sum_{s=a,b} \epsilon_s |s\rangle\langle s| + \tfrac{1}{2}\Delta\left(|a\rangle\langle b| + |b\rangle\langle a|\right), \tag{1a}$$

$$H_{\rm D} = \sum_{k\in{\rm L}} \varepsilon_k \hat{c}_k^\dagger \hat{c}_k + \sum_{q\in{\rm R}} \varepsilon_q \hat{c}_q^\dagger \hat{c}_q, \tag{1b}$$

$$H' = \sum_{s=a,b} \sum_{k,q} t_{kq}^s \hat{c}_k^\dagger \hat{c}_q \cdot |s\rangle\langle s| + {\rm H.c.} \tag{1c}$$

The amplitude $t_{kq}^s$ of electron tunneling through two reservoirs ($\alpha$ = L and R) of the QPC depends explicitly on the qubit state. Denote $Q_s \equiv |s\rangle\langle s|$ hereafter. Thus, the qubit–QPC

 

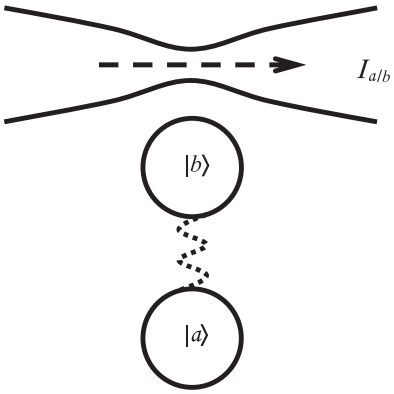


**Figure 1.** Schematic set-up of a solid-state charge qubit measured continuously by a quantum-point contact (QPC).

detector coupling in the $H_{\rm D}$-interaction picture is $H'(t) = \sum_s [\hat{f}_s(t) + \hat{f}_s^\dagger(t)]\cdot Q_s$, with $\hat{f}_s(t) \equiv {\rm e}^{{\rm i}H_{\rm D}t}(\sum_{kq} t_{kq}^s \hat{c}_k^\dagger \hat{c}_q){\rm e}^{-{\rm i}H_{\rm D}t}$. The effects of the stochastic QPC reservoirs on measurement are characterized by $\tilde{C}_{ss'}^{(+)}(t-\tau) \equiv \langle \hat{f}_s^\dagger(t)\, \hat{f}_{s'}(\tau)\rangle$ and $\tilde{C}_{ss'}^{(-)}(t-\tau) \equiv \langle \hat{f}_s(t)\, \hat{f}_{s'}^\dagger(\tau)\rangle$. In terms of the reservoir's spectral density functions, which are defined physically as

$$J_{ss'}(\omega,\omega') = \sum_{k,q} t_{kq}^s t_{kq}^{s'} \delta(\omega-\varepsilon_k)\delta(\omega'-\varepsilon_q), \tag{2}$$

these QPC coupling correlation functions are

$$\tilde{C}_{ss'}^{(\pm)}(t) = \int\int {\rm d}\omega\, {\rm d}\omega'\, J_{ss'}(\omega,\omega') f_{\rm L}^{(\pm)}(\omega) f_{\rm R}^{(\mp)}(\omega'){\rm e}^{{\rm i}(\omega-\omega')t}.$$

Here, $f_\alpha^{(\pm)}(\omega) = \{1+{\rm e}^{\pm\beta(\omega-\mu_\alpha)}\}^{-1}$ relates to the Fermi function of the lead $\alpha$, with $\beta = (k_{\rm B}T)^{-1}$ the inverse temperature. The coupling spectrum function used later is defined by

$$C_{ss'}^{(\pm)}(\omega) \equiv \int_{-\infty}^{\infty} {\rm d}t\, \tilde{C}_{ss'}^{(\pm)}(t){\rm e}^{-{\rm i}\omega t}. \tag{3}$$

Throughout this work, we set $\mu_{\rm L}^{\rm eq} = \mu_{\rm R}^{\rm eq} = 0$ for the equilibrium chemical potentials (or Fermi energies) of the QPC reservoirs in the absence of applied bias voltage and $\hbar = e = 1$ for the Planck constant and electron charge.

## 3. Particle-number-resolved master equation

The reduced density matrix of the qubit is formally defined as $\rho(t) \equiv {\rm Tr}_{\rm D}[\rho_{\rm T}(t)]$, i.e. tracing out the QPC reservoir's degree of freedom over the entire qubit-plus-detector density matrix. The qubit system Liouvillian is defined via $\mathcal{L}\hat{O} \equiv [H_{\rm qu}, \hat{O}]$. By treating $H'$ as a perturbation, a master equation for the reduced density matrix can be derived as [26, 27, 30]

$$\dot{\rho}(t) = -{\rm i}\mathcal{L}\rho(t) - \tfrac{1}{2}\sum_s [Q_s, \tilde{Q}_s\rho(t) - \rho(t)\tilde{Q}_s^\dagger], \tag{4}$$

with $\tilde{Q}_s \equiv \tilde{Q}_s^{(+)} + \tilde{Q}_s^{(-)}$ and

$$\tilde{Q}_s^{(\pm)} \equiv \sum_{s'} [C_{ss'}^{(\pm)}(\mathcal{L}) + i\, D_{ss'}^{(\pm)}(\mathcal{L})] Q_{s'}. \tag{5}$$

Here, $C_{ss'}^{(\pm)}(\mathcal{L}) \equiv C_{ss'}^{(\pm)}(\omega)|_{\omega=\mathcal{L}}$ is the spectrum function defined earlier. The dispersion function $D_{ss'}^{(\pm)}(\mathcal{L})$ can then be evaluated via the Kramers–Kronig relation:

$$D_{ss'}^{(\pm)}(\omega) = \frac{1}{\pi}\mathcal{P}\int_{-\infty}^{\infty} {\rm d}\omega'\, \frac{C_{ss'}^{(\pm)}(\omega')}{\omega-\omega'}. \tag{6}$$

Physically, it is responsible for the renormalization [26–29].

To achieve a description of the output from the detector, we employ the transport particle number '$n$'-resolved reduced density matrices $\{\rho^{(n)}(t); n = 0, 1, \ldots\}$ that satisfy $\rho(t) = \sum_n \rho^{(n)}(t)$. The corresponding '$n$'-resolved conditional quantum master equation is [8, 31, 32]

$$\dot{\rho}^{(n)}(t) = -{\rm i}\mathcal{L}\rho^{(n)}(t) - \tfrac{1}{2}\sum_s \{Q_s\tilde{Q}_s\rho^{(n)} - \tilde{Q}_s^{(-)}\rho^{(n-1)}Q_s - \tilde{Q}_s^{(+)}\rho^{(n+1)}Q_s + {\rm H.c.}\}. \tag{7}$$

We would like to account for the finite bandwidth of the QPC detector, which will be characterized by a single Lorentzian. Real spectral density has a complicated structure, which can be parameterized via the technique of spectral decomposition [33, 34]. This complexity, however, will only modify details of the results, but not the qualitative picture. For the sake of constructing analytical results, we assume a simple Lorentzian function centered at the Fermi energy for the spectral density (2). This choice stems also from the assumption that the energy band of each reservoir is half-filled. Moreover, the bias voltage is conventionally described by a relative shift of the entire energy bands, thus the centers of the Lorentzian functions would fix at the Fermi levels. Without loss of generality, we simply assume

$$J_{ss'}(\omega,\omega') = \mathcal{T}_s\mathcal{T}_{s'}\frac{\Gamma_{\rm L}^0 w^2}{(\omega-\mu_{\rm L})^2+w^2}\cdot\frac{\Gamma_{\rm R}^0 w^2}{(\omega'-\mu_{\rm R})^2+w^2}. \tag{8}$$

We set $\mathcal{T}_a \equiv 1$ and $\mathcal{T}_b \equiv 1-\chi$. The asymmetric qubit–QPC coupling parameter is of $0 < \chi < 1$, as inferred from figure 1. The correlation function of (3) can be evaluated as $C_{ss'}^{(\pm)}(\omega) = \mathcal{T}_s\mathcal{T}_{s'}C^{(\pm)}(\omega)$, with

$$C^{(\pm)}(\omega) = \frac{\eta g(x)}{1-{\rm e}^{\beta x}}\left[\frac{w^2}{x}\{\phi(0)-\phi(x)\} - \frac{w}{2}\varphi(x)\right]_{x=\omega\pm V}. \tag{9}$$

Here, $\eta = 2\pi\Gamma_{\rm L}^0\Gamma_{\rm R}^0$, $g(x) = 4w^2/(x^2+4w^2)$ and $V = \mu_{\rm L}-\mu_{\rm R}$ is the applied voltage on the QPC detector; $\phi(x)$ and $\varphi(x)$ denote the real and imaginary parts of the digamma function $\Psi(\frac{1}{2}+\beta\frac{w+{\rm i}x}{2\pi})$, respectively. Knowing the spectral function, the dispersion function $D_{ss'}^{(\pm)}(\omega) = \mathcal{T}_s\mathcal{T}_{s'}D^{(\pm)}(\omega)$ can be obtained via the Kramers–Kronig relation. The present spectrum functions satisfy the detailed-balance relation $C^{(+)}(\omega) = {\rm e}^{-\beta(\omega+V)}C^{(-)}(-\omega)$. This means that our approach properly accounts for the energy exchange between the qubit and the detector during measurement.

## 4. Output power spectral density

In continuous weak measurement of qubit oscillations, the most important output is the spectral density of the current.

Typically, the power spectrum is defined with a stationary state. The involving stationary state $\rho^{\rm st}$ can be determined by setting $\dot\rho^{\rm st} = 0$ in (4), together with the normalization condition, at a given bias voltage and temperature. For clarity, we focus hereafter on the symmetric qubit case, with the state energies of $\epsilon_a = \epsilon_b = 0$.

Let us start with the average current. Using the '$n$'-resolved master equation (7), the average current can be expressed as $I(t) = \sum_n n\,{\rm Tr}[\dot\rho^{(n)}(t)] = {\rm Tr}[\mathcal{J}^{(-)}\rho(t)]$, where $\mathcal{J}^{(-)}$ is one of the superoperators, defined as

$$\mathcal{J}^{(\pm)}\rho(t) \equiv \tfrac{1}{2}\sum_s (\tilde Q_s^{(-)} \pm \tilde Q_s^{(+)})\rho(t)Q_s + {\rm H.c.} \tag{10}$$

The stationary current can be carried out as

$$\bar I = I_a\rho_{aa}^{\rm st} + I_b\rho_{bb}^{\rm st} + I_{ab}\rho_{ab}^{\rm st}, \tag{11}$$

which for a symmetric qubit ($\epsilon_a = \epsilon_b = 0$) is of

$$\begin{aligned} I_a &= \left(1-\frac{\chi}{2}\right)C(0)\tanh\left(\frac{\beta V}{2}\right) + \chi\bar\gamma_+,\\ I_b &= (1-\chi)\left[\left(1-\frac{\chi}{2}\right)C(0)\tanh\left(\frac{\beta V}{2}\right) - \chi\bar\gamma_+\right],\\ I_{ab} &= \chi^2\bar\gamma_-. \end{aligned} \tag{12}$$

Here, $\bar\gamma_\pm \equiv \frac{1}{4}[\bar C(\Delta) \pm \bar C(-\Delta)]$, with $\bar C(\omega) \equiv C^{(-)}(\omega) - C^{(+)}(\omega)$. Denote also $C(\omega) \equiv C^{(-)}(\omega) + C^{(+)}(\omega)$.

The noise spectral density can be calculated via MacDonald's formula [35]:

$$S(\omega) = 2\omega\int_0^\infty {\rm d}t\,\sin(\omega t)\frac{\rm d}{{\rm d}t}[\langle n^2(t)\rangle - (\bar I t)^2], \tag{13}$$

with $\langle n^2(t)\rangle \equiv \sum_n n^2\,{\rm Tr}\{\rho^{(n)}(t)\}$. Applying equation (7) gives

$$\frac{\rm d}{{\rm d}t}\langle n^2(t)\rangle = {\rm Tr}[2\mathcal{J}^{(-)}N(t) + \mathcal{J}^{(+)}\rho^{\rm st}], \tag{14}$$

where $N(t) \equiv \sum_n n\rho^{(n)}(t)$, which can be calculated via

$$\frac{{\rm d}N}{{\rm d}t} = -{\rm i}\mathcal{L}N - \frac{1}{2}\sum_s\left[Q_s,\,\tilde Q_s N - N\tilde Q_s^\dagger\right] + \mathcal{J}^{(-)}\rho(t). \tag{15}$$

For a symmetric qubit, an analytical result is available. We split the spectrum into four components, $S = S_0 + S_1 + S_2 + S_3$, and present them one by one as follows. First, the frequency-independent background noise $S_0$ is

$$\begin{aligned} S_0 = {}& 2\bar I\coth\left(\frac{\beta V}{2}\right) - \chi^2(\gamma_-/\gamma_+)\left[\gamma_- - \bar\gamma_-\coth\left(\frac{\beta V}{2}\right)\right]\\ &+ \chi[\chi - (2-\chi)\delta\bar P]\left[\gamma_+ - \bar\gamma_+\coth\left(\frac{\beta V}{2}\right)\right], \end{aligned} \tag{16}$$

with $\gamma_\pm \equiv \frac{1}{4}[C(\Delta) \pm C(-\Delta)]$ and $\delta\bar P \equiv \rho_{bb}^{\rm st} - \rho_{aa}^{\rm st}$ which is nonzero due to the asymmetric qubit–QPC coupling. The second component is a Lorentzian, with the peak at $\omega = 0$ and the dephasing rate of $\gamma_{\rm d} = \chi^2\gamma_+$. It is

$$S_1 = (X\gamma_{\rm d} - \chi^2\gamma_-\bar I)\frac{2I_{ab}}{\omega^2 + \gamma_{\rm d}^2}. \tag{17}$$

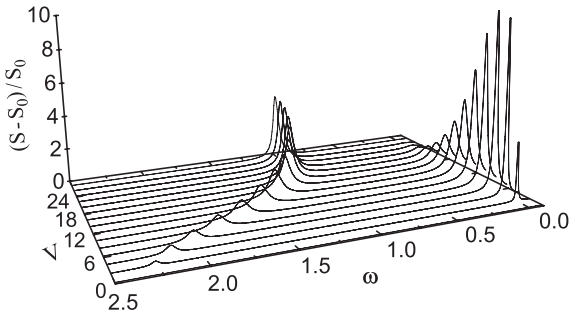


**Figure 2.** Power spectral density of the detector current, with the frequency and voltage labeled in units of $\Delta$. The bandwidth $w = 15\Delta$. Other parameters are $\eta = 2$, $\chi = 0.2$ and $\beta\Delta = 1$.

Here, $2\langle a|\mathcal{J}^{(+)}\rho^{\rm st}|b\rangle \equiv X + {\rm i}Y$ (the real and imaginary parts). We remark that $S_1$ arises completely from the qubit relaxation-induced inelastic tunneling effect in the detector [8]. The last two components are

$$S_2 = \left[\frac{(\chi^2\gamma_-\bar I - X\gamma_{\rm d})\tilde\epsilon}{\omega^2+\gamma_{\rm d}^2} + Y\right]\frac{\omega^2\gamma_{\rm d}'A - (\omega\omega' - \Delta\tilde\Delta)B}{\omega^2\gamma_{\rm d}'^2 + (\omega\omega' - \Delta\tilde\Delta)^2}, \tag{18}$$

$$S_3 = \left[\frac{(\chi^2\gamma_-\bar I\gamma_{\rm d} + X\omega^2)\tilde\epsilon}{\omega^2+\gamma_{\rm d}^2} - \Delta Z\right]\frac{\gamma_{\rm d}'B - (\omega\omega' - \Delta\tilde\Delta)A}{\omega^2\gamma_{\rm d}'^2 + (\omega\omega' - \Delta\tilde\Delta)^2}. \tag{19}$$

Here, $\tilde\epsilon$ and $\tilde\Delta$ are the renormalized version of the original $\epsilon \equiv \epsilon_a - \epsilon_b$ and $\Delta$ of the qubit. They are related to the dispersion functions of the detector. Let $D(\omega) \equiv D^{(-)}(\omega) + D^{(+)}(\omega)$ and $\bar D(\omega) \equiv D^{(-)}(\omega) - D^{(+)}(\omega)$. Simple analysis on the symmetric case ($\epsilon = 0$) gives

$$\tilde\epsilon = \chi\left(1-\frac{\chi}{2}\right)D(0), \tag{20a}$$

$$\tilde\Delta = \Delta + \tfrac{1}{4}\chi^2[D(\Delta) - D(-\Delta)]. \tag{20b}$$

For the bookkeeping of (18) and (19), we have also introduced $Z \equiv \frac{1}{2}[(I_a + I_b)\delta\bar P + (I_a - I_b)] + (\frac{2}{\chi} - 1)I_{ab}\rho_{ab}^{\rm st}$, and the frequency-dependent quantities of

$$\begin{aligned} \omega' &\equiv \omega\left(1 - \frac{\tilde\epsilon^2}{\omega^2+\gamma_{\rm d}^2}\right), \qquad \gamma_{\rm d}' \equiv \gamma_{\rm d}\left(1 + \frac{\tilde\epsilon^2}{\omega^2+\gamma_{\rm d}^2}\right),\\ A &\equiv \chi\left(1-\frac{\chi}{2}\right)[\bar D(\Delta) - \bar D(-\Delta)] + 2\tilde\epsilon I_{ab}\frac{\gamma_{\rm d}^2}{\omega^2+\gamma_{\rm d}^2},\\ B &\equiv -2(I_a - I_b)\Delta + 2\tilde\epsilon I_{ab}\frac{\omega^2}{\omega^2+\gamma_{\rm d}^2}. \end{aligned} \tag{21}$$

The computed noise spectrum is displayed in figure 2. It is of interest to note that the spectral peak, apart from the zero frequency, which is the signal of qubit oscillations, shifts with the measurement voltages. (i) In the high voltage regime (e.g. for $V \gtrsim 30\,\Delta$ as shown in figure 2), the oscillation peak is located approximately at $\omega \approx \Delta$; (ii) on lowering the voltage, the measurement-induced renormalization effect becomes increasingly important, which strongly affects the position of the oscillation peak.

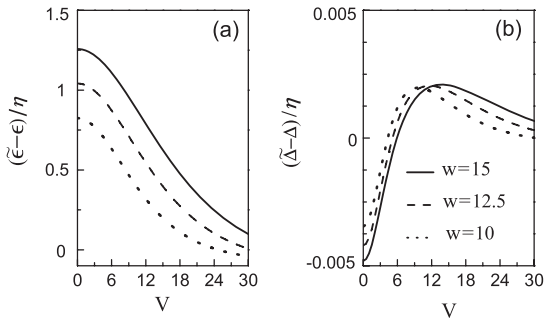


**Figure 3.** Renormalization on the qubit level energy (a) and coupling (b), exemplified by three values of bandwidth $w$ (in units of $\Delta$). Other parameters are the same as in figure 2.

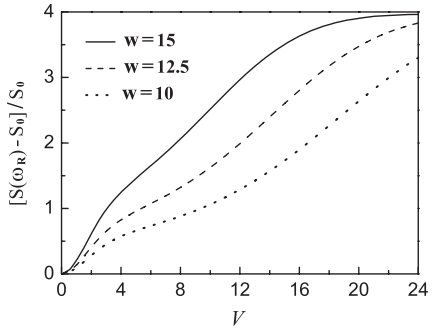


**Figure 4.** Bias voltage dependence of the peak-to-pedestal ratio of the output power spectrum, exemplified with the same parameters in figure 3.

The feature of the noise spectrum in figure 2 is closely related to the renormalization of the qubit parameters $\epsilon$ and $\Delta$. In the limit of weak qubit–QPC coupling, the renormalized Rabi frequency is given by $\omega_R = \sqrt{\tilde{\epsilon}^2 + \tilde{\Delta}^2}$. The renormalization effect $(\omega_R - \sqrt{\epsilon^2 + \Delta^2})$ increases *monotonically* with the QPC bandwidth $(w)$. In figure 3 we plot $\tilde{\epsilon}$ and $\tilde{\Delta}$, in terms of the $\eta$-scaled renormalizations, against the bias voltage for different bandwidths. The renormalized qubit state energy difference $\tilde{\epsilon}$ increasingly deviates from the original $\epsilon = 0$ as the QPC bandwidth increases or the applied voltage decreases, as shown in figure 3(a). In contrast, the inter-state coupling renormalization is negligibly small, as depicted in figure 3(b) and also claimed in [25]. That $(\tilde{\epsilon} - \epsilon)$ being dominant can be readily understood by the form of coupling $H'$ of (1*c*), which modulates the level energies, rather than the level coupling. In the wide-band limit $(w \to \infty)$, the energy renormalization would diverge. However, this feature is an artifact, since in reality a natural cutoff of the bandwidth must exist. That is the reason we introduce a Lorentzian cutoff in (8).

The noise spectrum itself depends on $\eta$ in a rather complicated manner, especially the $S_2$ and $S_3$ components ((18) or (19) with (21)) that are dynamical in nature. In contrast, the algebraic nonlinear dependence of $\eta$ in the average current $\bar{I}$ (11) and $S_0$ (16) arises from the renormalized stationary $\rho^{st}$ only. In the literature (e.g. [25]) the dispersion function is often disregarded explicitly, with its effect being included in the Caldeira–Leggett renormalized system Hamiltonian [26–29]. However, this approach gives rise to quite different dynamics from the present result, even though their stationary state behaviors could be similar [26, 27]. Apparently, the dynamic distinction should be sensitively reflected in the shot noise spectrum. In the context of qubit measurement by a QPC detector, our analysis can serve as a detailed investigation of the dynamical renormalization effect.

In figure 4 we further show the signal-to-noise ratio of the noise spectrum against the bias voltage for different bandwidths. In the limit of large bias $V \gg \Delta$ and for weak qubit–QPC coupling, the signal-to-noise ratio

$$\left.\frac{S(\omega_R) - S_0}{S_0}\right|_{V\gg\Delta} \to 4\,\frac{(2-\chi)^2}{(2-\chi)^2 + \chi^2} \tag{22}$$

can reach the limit of 4, i.e. the Korotkov–Averin bound for any linear response detectors [3, 36–38].

As seen in figure 2, the detector-induced renormalization also results in a wide voltage range where the coherent peak at the renormalized Rabi frequency and the sharp peak at zero frequency coexist. In that regime, the level mismatch induced by the detector is prominent, while the qubit coherence is not strongly destroyed. As is well known [3, 25, 39], the peak at zero frequency is a signature of the Zeno effect in continuous weak measurement. The basic picture is that the detector attempts to localize the electron in one of the levels for a longer time, leading thus to incoherent jumps between the two levels. Finally, in figure 2, the coherent peak persists to high bias voltage, while the zero frequency peak eventually disappears. This feature is different from the previous work [8]. The reason is twofold. On the one hand, as shown in figure 3, the renormalization of energy levels is weak at high voltage. On the other hand, in this work we adopted a finite bandwidth model for the QPC. This implies that in the high voltage regime the QPC (measurement) current is weak, which differs from the result under the usual wide-band approximation. As a consequence, the weak backaction from the detector together with the alignment of the qubit levels results in the spectral feature shown in figure 2 at high voltages.

## 5. Conclusions

In summary, we have revisited the problem of continuous measurement of a solid-state qubit by quantum point contact. Our results showed that the renormalization effect, which was neglected in previous studies, can significantly affect the output power spectrum. This feature should be taken into account in the interpretation of measurement result. We also note that the renormalization in the present set-up may be quantified *in situ*. No reference to the bare qubit is needed, as it can be effectively replace the band-edge large voltage transport limit.

## Acknowledgments

This work is supported by RGC (604007 and 604508) of the Hong Kong SAR Government, the National Natural Science Foundation (60425412 and 90503013) and the Major State Basic Research Project (2006CB921201) of China.

## References


[1] Aleiner I L, Wingreen N S and Meir Y 1997 *Phys. Rev. Lett.* **79** 3740
[2] Gurvitz S A 1997 *Phys. Rev.* B **56** 15215
[3] Korotkov A N and Averin D V 2001 *Phys. Rev.* B **64** 165310
[4] Goan H S, Milburn G J, Wiseman H M and Sun H B 2001 *Phys. Rev.* B **63** 125326
[5] Averin D V and Sukhorukov E V 2005 *Phys. Rev. Lett.* **95** 126803
[6] Pilgram S and Büttiker M 2002 *Phys. Rev. Lett.* **89** 200401
[7] Clerk A A, Girvin S M and Stone A D 2003 *Phys. Rev.* B **67** 165324
[8] Li X Q, Cui P and Yan Y J 2005 *Phys. Rev. Lett.* **94** 066803
[9] Shnirman A and Schön G 1998 *Phys. Rev.* B **57** 15400
[10] Devroret M H and Schoelkopf R J 2000 *Nature* **406** 1039
[11] Makhlin Y, Schön G and Shnirman A 2001 *Rev. Mod. Phys.* **73** 357
[12] Clerk A A, Girvin S M, Nguyen A K and Stone A D 2002 *Phys. Rev. Lett.* **89** 176804
[13] Jiao H, Li X Q and Luo J Y 2007 *Phys. Rev.* B **75** 155333
[14] Gilad T and Gurvitz S A 2006 *Phys. Rev. Lett.* **97** 116806
[15] Gurvitz S A and Berman G P 2005 *Phys. Rev.* B **72** 073303
[16] Oxtoby N P, Wiseman H M and Sun H B 2006 *Phys. Rev.* B **74** 045328
[17] Buks E, Schuster R, Heiblum M, Mahalu D and Umansky V 1998 *Nature* **391** 871
[18] Schoelkopf R J, Wahlgren P, Kozhevnikov A A, Delsing P and Prober D E 1998 *Science* **280** 1238
[19] Nakamura Y, Pashkin Y A and Tsai J S 1999 *Nature* **398** 786
[20] Sprinzak D, Buks E, Heiblum M and Shtrikman H 2000 *Phys. Rev. Lett.* **84** 5820
[21] Aassime A, Johansson G, Wendin G, Schoelkopf R J and Delsing P 2001 *Phys. Rev. Lett.* **86** 3376
[22] Elzerman J M, Hanson R, van Beveren L H W, Witkamp B, Vandersypen L M K and Kouwenhoven L P 2004 *Nature* **430** 431
[23] Trauzettel B, Jordan A N, Beenakker C W J and Büttiker M 2006 *Phys. Rev.* B **73** 235331
[24] Schomerus H and Robinson J P 2007 *New J. Phys.* **9** 67
[25] Shnirman A, Mozyrsky D and Martin I 2002 *LANL preprint* arXiv:cond-mat/0211618
[26] Xu R X and Yan Y J 2002 *J. Chem. Phys.* **116** 9196
[27] Yan Y J and Xu R X 2005 *Annu. Rev. Phys. Chem.* **56** 187
[28] Caldeira A O and Leggett A J 1983 *Physica* A **121** 587
[29] Weiss U 2008 *Quantum Dissipative Systems* 3rd edn (Singapore: World Scientific)
[30] Yan Y J 1998 *Phys. Rev.* A **58** 2721
[31] Li X Q, Luo J Y, Yang Y G, Cui P and Yan Y J 2005 *Phys. Rev.* B **71** 205304
[32] Luo J Y, Li X Q and Yan Y J 2007 *Phys. Rev.* B **76** 085325
[33] Meier C and Tannor D J 1999 *J. Chem. Phys.* **111** 3365
[34] Li X Q and Yan Y J 2007 *Phys. Rev.* B **75** 075114
[35] MacDonald D K C 1962 *Noise and Fluctuations: an Introduction* (New York: Wiley) chapter 2.2.1
[36] Korotkov A N 2001 *Phys. Rev.* B **63** 085312
[37] Averin D V and Korotkov A N 2005 *Phys. Rev. Lett.* **94** 069701
[38] Jiao H, Wang S K, Li F and Li X Q 2008 arXiv:0806.2502
[39] Gurvitz S A, Fedichkin L, Mozyrsky D and Berman G P 2003 *Phys. Rev. Lett.* **91** 066801